Combined FRM and GDFT filter bank designs for improved non-uniform DSA channelization

Álvaro Palomo-Navarro, Ronan J. Farrell, Rudi Villing
Callan Institute for Applied ICT, Electronic Engineering Department,
National University of Ireland Maynooth, Maynooth, Co. Kildare, Ireland
Email: {apalomo, ronan.farrell, rudi.villing}@eeng.nuim.ie

ABSTRACT

Multi-standard channelization for base stations is a big application of Generalised Discrete Fourier Transform Modulated Filter Banks (GDFT-FB) in digital communications. For technologies such as Software-Defined Radio (SDR) and Cognitive Radio (CR), non-uniform channelizers must be used if frequency bands are shared by different standards. However, GDFT-FB based non-uniform channelizers can suffer from high filter orders when applied to wideband input signals. In this paper various combinations of GDFT-FB with the Frequency Response Masking (FRM) technique are proposed and evaluated for both uniform and non-uniform channelization applications. Results show that the proposed techniques achieve savings in both the number of filter coefficients and the number of operations per input sample.

KEYWORDS

Frequency response masking; generalised discrete Fourier transform modulated filter banks; uniform channelization; non-uniform channelization; dynamic spectrum allocation.

I. INTRODUCTION

Modulated filter banks have gained importance in digital communications because of their application to multi-carrier modulation techniques and channelizers for base stations [1, 2]. In the latter application, channelization implies the extraction of independent channels contained in the received uplink signal by bandpass filtering and down-converting them prior to subsequent baseband processing of each channel independently. Modulated filter banks eliminate the need for an independent low-pass or band-pass filter to isolate

each information channel, replacing them with a single low-pass *prototype filter* and an efficient modulation operation that can filter multiple channels at once. As a result, the computational load of the channelization is shared among multiple channels, and does not increase linearly with the number of channels.

Recent trends in wireless communications such as Software-Defined Radio (SDR) [3] and Cognitive Radio (CR) [4] make use of Dynamic Spectrum Allocation (DSA) techniques to make more efficient use of the radio communications spectrum [5, 6]. With DSA the same frequency band may be shared by different wireless standards with different channel properties. Some of the advantages of DSA are an efficient utilisation of some frequency bands, better electromagnetic propagation properties, and the provision of new capabilities to existing standards. Nevertheless, the differing characteristics of channels sharing the frequency band requires that the DSA compliant base station employs *non-uniform* channelization to separate the independent information channels [7].

Non-uniform channelization techniques have been proposed based on Discrete Fourier Transform Modulated Filter Banks (DFT-FB) [8-11] and other techniques including Farrow Per-Channel Channelizers (FPCC) [12] and Frequency Response Masking based Filter Banks (FRM-FB) [13, 14]. Of these, only the DFT-FBs can take advantage of modulated filter bank properties in order to minimize the computational load in a base station channelizer processing a large number of channels in the uplink signal. In addition, FRM-FBs suffer from large group delays due to the interpolation factors applied to the filters.

Unfortunately, DFT-FB based uniform and non-uniform channelizers encounter problems related to the prototype filter order required, particularly when narrowband channels must be channelized [8]. Some solutions have been proposed to reduce the prototype filter order in complex modulated filter banks. For example, a multi-stage filtering design may be used

in which a Generalized DFT-FB (GDFT-FB) cascaded with a set of half-band filters progressively carries out the sub-band filtering [3]. This reduces the prototype filter order and number of operations per input sample required. In other cases, the effort has been focused on designing multiplier-less DFT-based filter banks.

This paper presents two further approaches to reduce the number of filter coefficients and computational load required by a GDFT-FB based channelizer (uniform or non-uniform) by combining the Frequency Response Masking (FRM) technique with classic GDFT-FB designs. In the first approach, a hybrid filtering design is formed by an FRM front-end and a GDFT-FB back-end. In the second approach, FRM is used to directly optimize the GDFT-FB filter implementation (based on a similar approach previously applied to real cosine modulated filter banks [15-18]). Both approaches reduce the number of prototype filter coefficients and the number of operations per input sample for the price of increasing the group delay introduced by the channelizer. In particular, Section II presents the Hybrid GDFT-FB design (H-GDFT) while Section III covers a number of different direct FRM GDFT-FB designs. In addition, Section II describes two different structures for non-uniform channelization based on uniform filter banks. Section IV shows the filter design and computational advantages of the designs proposed in the paper when applied to non-uniform channelization and DSA. Finally, Section V analyses and summarizes the conclusions derived from the content of this paper.

II. HYBRID GDFT-FB

The FRM technique is based on two particular filtering techniques: linear interpolation of filters and multi-stage filtering [19]. The FRM structure is divided into two branches known as *positive* (top) and *complementary* (bottom) as shown in Figure 1a. The positive branch is formed by cascading the base filter, $H_a(z)$, and the positive masking filter, $H_{Ma}(z)$.

The complementary branch is formed by the complementary filter, $H_c(z)$, cascaded with the complementary masking filter, $H_{Mc}(z)$.

The transfer function of the structure is given by

$$H(z) = H_a(z^L)H_{Ma}(z) + H_c(z^L)H_{Mc}(z) \tag{1}$$

An alternative FRM structure, that exploits the complementary relationship between $H_a(z)$ and $H_c(z)$, requires only three filters as shown in Figure 1b, where N_a represents the order of $H_a(z)$. For certain applications where a very narrow filter passband is required, only the positive branch is used. This case is generally known as *narrowband* FRM, as opposed to the more general case or *full* FRM [19]. In the narrowband case (1) is reduced to

$$H(z) = H_a(z^L)H_{Ma}(z) \tag{2}$$

Finally, if the condition is imposed that both the base and complementary filter have the same passband and transition band widths, then the base filter must be designed with its transition band centred at $\pi/2$ rad, that is, as a half-band filter [20]. The use of half-band filters provides additional advantages since roughly half of their coefficients are equal to zero, making them computationally efficient, and their frequency response is naturally magnitude complementary without requiring any coefficient optimisation process. Consequently, the relationship between base and complementary filters can be expressed as

$$H_c(z) = H_a(-z) \tag{3}$$

which means that both filters share the same polyphase components:

$$H_a(z) = H_{a0}(z^2) + z^{-1}H_{a1}(z^2) \tag{4}$$

$$H_c(z) = H_{c0}(z^2) + z^{-1}H_{c1}(z^2) = H_{a0}(z^2) - z^{-1}H_{a1}(z^2) \tag{5}$$

Based on (4) and (5), the FRM implementation in Figure 1c is obtained where the

complementary filter is implemented as a mirror image sum and difference [21].

Based on the desired passband (ω_p) and stopband (ω_s) cut-off frequencies of the FRM filter response Table 1 shows how to calculate appropriate passband and stopband frequencies for the individual base and masking filters. For full FRM there are two design cases: in case 1 the FRM filter transition band is given by an interpolated image of the base filter, whereas in case 2 the FRM filter transition band is given by an interpolated image of the complementary filter. Since there is no complementary filter used in narrowband FRM, there is only one possible design case. For the case 1 and case 2 the value of *m* is given by

$$\begin{aligned} &\text{Case 1: } m = \lfloor \omega_p L / 2\pi \rfloor \\ &\text{Case 2: } m = \lceil \omega_s L / 2\pi \rceil \end{aligned} \tag{6}$$

where $\lfloor \omega_p L / 2\pi \rfloor$ denotes the largest integer smaller than $\omega_p L / 2\pi$, and $\lceil \omega_s L / 2\pi \rceil$ denotes the smallest integer bigger than $\omega_s L / 2\pi$.

Channelizer designs using FRM have been previously proposed for SDR applications, notably the FRM based filter bank (FRM-FB) and the coefficient decimation filter bank (CDFB) [13]. In the FRM-FB, the base and complementary filters are designed so that their images after interpolation meet the required channel passband and transition band specifications. The masking filters, comprising a real lowpass filter, a real highpass filter, and *L*-2 complex bandpass filters, are then designed to extract individual channels. Unlike uniform modulated filter banks such as the GDFT-FB, the base and masking filters in the FRM-FB both work at the high input sample rate of the wideband multi-channel signal. Although the design of the masking filters is simplified and the number of coefficients reduced by the use of FRM, the high sample rate of the input signal can often result in more operations per second than a GDFT-FB design.

*A. **Hybrid combination of FRM and GDFT-FBs***

We propose an improvement to the FRM-FB by replacing the set of individual masking filters with two GDFT-FBs as shown in Figure 2a. The GDFT-FBs, whose general structure is shown in Figure 2b, replace the set of masking filters in the positive and complementary branches respectively. For GDFT-FBs as in other modulated filter banks, a set of K bandpass filters $H_k(z)$ are generated from a lowpass prototype filter $H(z)$ as

$$H(z) = \sum_{p=0}^{K-1} z^{-p} E_p(z^K) \tag{7}$$

$$H_k(z) = W_K^{-(k+k_0)n_0} \sum_{p=0}^{K-1} z^{-p} W_K^{-kp} W_K^{-k_0 p} E'_p(z^K) \tag{8}$$

with

$$E'_p(z^K) = E_p(z^K W_K^{-k_0 D}) \tag{9}$$

where $W_K = e^{j2\pi/K}$, $E_p(z)$ are the K polyphase components of the prototype filter, D is the decimation factor, n_0 is a possible phase shift which can be applied to the filter bank outputs (in general $n_0 = 0$), and k_0 determines the *even* or *odd* stacking of the filter bank sub-bands ($k_0 = 0$ for even stacked and $k_0 = ½$ for odd stacked). L_{DFT} is the oversampling factor of the GDFT-FB which is defined as

$$L_{DFT} = \frac{K}{D} \tag{10}$$

When $L_{DFT} = 1$ the GDFT-FB is called *critically sampled*, whereas when $L_{DFT} > 1$ it is called *oversampled*.

In contrast to the masking filters of the FRM-FB, each GDFT-FB requires just one prototype filter and works at a lower sample rate resulting from its internal decimation

operations. This hybrid of the FRM-FB and GDFT-FB is called the Hybrid GDFT-FB (H-GDFT). In the H-GDFT, as in the FRM-FB, the interpolated versions of the base filter and complementary filter each extract half of the wideband input signal channels: the even and odd channels respectively.

To ensure that base and complementary filter images have the same passband and transition band widths, the base filter is designed as a half-band filter with its transition band centred at $\pi/2$ rad, as shown in Figure 3a.

The interpolation factor of the base half-band filter, L, is determined by the number of sub-bands of the GDFT-FBs according to

$$L = \frac{K}{2} \tag{11}$$

where K is the number of sub-bands in the GDFT-FBs. Therefore, considering the desired final frequency response passband (ω_p) and stopband (ω_s) cut-off frequencies, the FRM base filter passband (θ) and stopband (ϕ) specifications are given by

$$\theta = \omega_p L \tag{12}$$

$$\phi = \omega_s L \tag{13}$$

The initial filtering performed by the base and complementary filters yields two multi-channel signals, $w_a(n)$ and $w_c(n)$ in Figure2 and Figure 3, each of which contains a null for every second channel. This benefits the prototype filter design of the masking GDFT filter banks in two ways. First, each GDFT-FB can be critically sampled because of reduced aliasing from adjacent bands. Second, the transition band constraints of the GDFT-FB prototype filters can be relaxed (relative to a design without the base and complementary pre-filters) thereby reducing its order. Specifically, the GDFT-FB prototype

filters can be designed with a less sharp transition band between π/K and $2\pi/K$ rad.

Figure 3b-e show the two-stage filtering operation for the positive and complementary branch of the H-GDFT. For both of them, the first stage is the same as in the FRM-FB, with the images of the interpolated base (Figure 3b) and complementary (Figure 3d) filters selecting the set of even and odd channels respectively. In the second stage, the bandpass filters formed by each of the GDFT-FBs cascaded with the base (Figure 3c) and complementary (Figure 3e) filters extract the individual channels from $w_a(n)$ and $w_c(n)$ respectively.

To ensure that both the base and complementary filter images are centred exactly at the same centre frequencies as the GDFT-FBs sub-bands, the input sample rate of the multi-channel signal needs to satisfy

$$f_S = K \cdot f_{CS} \tag{14}$$

where f_{CS} represents the desired sub-band channel spacing.

Since half of the sub-bands are null (unused) in each GDFT-FB, further reductions in channelizer computation can be achieved. If only every I-th sub-band of a GDFT-FB is employed to receive information, a K-point DFT or FFT operation can be replaced by a (K/I)-point DFT or FFT [1].

The only condition that has to be met is that K is an integer multiple of I as

$$K = Q \cdot I \tag{15}$$

Since only Q of the output sub-bands are needed, then only Q of the DFT input samples have to be computed. Figure 4 shows a GDFT-FB design where each $s_q(n)$ signal is created as a *time aliased* version of a number I of $r_k(n)$ signals [1]. The time aliased signal is obtained according to

$$s_q(n) = \sum_{i=0}^{I-1} r_{q+Qi}(n) \quad 0 \le q \le Q-1 \tag{16}$$

As a result only the sub-bands containing actual information channels are processed by the DFT (or FFT).

In the particular case of the H-GDFT, $I = 2$ since only every second sub-band is effectively used. Therefore, the *K*-point DFT operations in each GDFT-FB in Figure 2a can be replaced by a *K*/2-point (or *Q*-point) DFT. Consequently, the computation of the null sub-bands is saved leading to the more efficient implementation.

*B. **Filter design example***

Using the GDFT-FB designs for TETRA V&D and TEDS channels from [3], the theoretical prototype filter orders required for GDFT-FB and H-GDFT designs are compared in Table 2. As in [3], the prototype filters were designed as FIR optimum equiripple filters with orders estimated using Kaiser's equation for equiripple filters [22].

Although the H-GDFT designs are composed of two filtering stages instead of one in the GDFT-FB, the base (N_a) and prototype filters (N) have a much larger transition band thereby reducing the number of coefficients by between 76.7% and 83.2%.

In addition, Table 2 shows the group delay expressed in number of output samples for both channelizer designs. This group delay is affected by the filter bank decimation factor, and consequently varies for critically sampled and oversampled configurations, as shown in the table. When translated into a time delay by multiplying the number of output samples by the output sample period, both of them become equal since the output sample period of the oversampled channelizer is half of the period of the critically sampled channelizer.

Although the H-GDFT requires a smaller number of coefficients, the large interpolation factors applied to the base filter in this design example leads to larger group delays than the

GDFT-FB, and consequently longer transient responses. Generally the length of the transient response of an FIR filter is not relevant in the field of communications, however, the time delay associated with it will contribute to the overall latency in the signal path, and therefore should be considered for real-time or delay-sensitive services.

To examine frequency response differences between the GDFT-FB and H-GDFT channelizers both methods where used to design an oversampled ($L_{DFT} = 2$) channelizer for eight TETRA V&D 25 kHz channels. The theoretical filter orders for the optimum equiripple designs were $N = 253$ for the GDFT-FB and N_a=64 and N=42 for the H-GDFT. Note that this is not a constraint and any desired digital filter design process could be used for the prototype filter, e.g. window method [20]. Due to aliasing effects [23], the filter orders had to be increased to N=280 for GDFT-FB and N_a=70 and N=52 for the H-GDFT in order to meet the filtering specifications in [3].

Figure 5a shows the magnitude response of the two designs, whereas Figure 5b focuses on the passband ripple. In the stopband, the H-GDFT response decreases with increasing frequency and this reduces the adjacent channel interference in comparison with the almost constant ripple of the GDFT-FB design. In the passband the magnitude response of the two channelizers also differs despite equiripple filter designs being used for all filters. The H-GDFT passband response exhibits non-uniform ripple caused by the cascading of several filters in its implementation. Nevertheless the passband ripple and stopband attenuation specifications are still met.

III. FRM GDFT-FB

An alternative approach to integrating FRM with the GDFT-FB is to directly apply FRM to the prototype filter implementation. Previous researchers have applied the FRM technique to the prototype filter design of cosine modulated filter banks for cases where

real signals are processed [15-17]. However, FRM has not been applied in this way to complex valued signals and in particular it has not been applied to complex modulated filter banks. Therefore we next extend the approach taken in the combined FRM and cosine modulated filter bank design [17] to complex signals and the GDFT-FB.

Substituting (4) and (5) into (1), the prototype filter $H(z)$ can be expressed as

$$H(z) = H_{a0}(z^{2L})H_{Ma}(z) + z^{-L}H_{a1}(z^{2L})H_{Ma}(z) + H_{a1}(z^{2L})H_{Mc}(z) - z^{-L}H_{a1}(z^{2L})H_{Mc}(z) \quad (17)$$

Identifying the common components in (17), this can be rearranged as

$$\begin{aligned} A(z) &= H_{Ma}(z) + H_{Mc}(z) \\ B(z) &= H_{Ma}(z) - H_{Mc}(z) \end{aligned} \quad (18)$$

$$H(z) = H_{a0}(z^{2L})A(z) + z^{-L}H_{a1}(z^{2L})B(z) \quad (19)$$

In addition, the polyphase decomposition can be applied to the masking filters to yield

$$\begin{aligned} A(z) &= \sum_{i=0}^{K-1} z^{-i}E_{Ai}(z^K) \\ B(z) &= \sum_{i=0}^{K-1} z^{-i}E_{Bi}(z^K) \end{aligned} \quad (20)$$

where $E_{Ai}(z)$ and $E_{Bi}(z)$ are the K polyphase components of $A(z)$ and $B(z)$ respectively.

The GDFT-FB modulated bandpass filters may be created from the lowpass prototype by application of the complex modulation in (9)

$$\begin{aligned} H_k(z) &= H_{a0}(z^{2L})A_k(z) + z^{-L}H_{a1}(z^{2L})B_k(z) \\ A_k(z) &= A(zW_K^{k+k_0}) \\ B_k(z) &= B(zW_K^{k+k_0}) \end{aligned} \quad (21)$$

Finally, each of the modulated bandpass filters is given by

$$H_k(z) = H_{a0}(z^{2L})\sum_{i=0}^{K-1} z^{-i}W_K^{-ki}W_K^{-k_0 i}E'_{Ai}(z^K) + (-1)^k z^{-L}H_{a1}(z^{2L})\sum_{i=0}^{K-1} z^{-i}W_K^{-ki}W_K^{-k_0 i}E'_{Bi}(z^K) \quad (22)$$

where

$$E'_{Ai}(z^K) = E_{Ai}(z^K W_K^{-k_0 D})$$
$$E'_{Bi}(z^K) = E_{Bi}(z^K W_K^{-k_0 D}) \tag{23}$$

The resulting FRM GDFT-FB structure is shown in Figure 6. For the outputs with odd indexes (k =1,3,…, K-1) there is a phase difference of π rad between the two polyphase components $E'_{Ai}(z^K)$ and $E'_{Bi}(z^K)$ in (22) as in [17]. Therefore, a phase rotation must be applied to the $w_k(n)$ signals with odd indexes as shown in Figure 6. For the odd stacked configuration, it is necessary to make k_0 = ½ and, at design time, to shift the frequency response of the base filter to be centred at π/2 rad.

Given the desired passband and stopband cut-off specifications for the prototype filter (ω_p and ω_s), the base and masking filters are designed using the expressions in Table 1. In addition, the value of the FRM interpolation factor is chosen according to

$$\text{Case 1: } L = (4m+1)\frac{K}{2}$$
$$\text{Case 2: } L = (4m-1)\frac{K}{2} \tag{24}$$

where m is any integer equal to or greater than 1.

*A. **Narrowband FRM GDFT-FB***

The FRM GDFT-FB structure in Figure 6 can be adapted for cases where a narrowband prototype filter is appropriate by only employing the FRM positive branch. For this case, (18) simplifies to

$$A(z) = B(z) = H_{Ma}(z) \tag{25}$$

Therefore, the prototype filter and the polyphase decomposition of the positive masking filter are given by

$$H(z) = H_{a0}(z^{2L})H_{Ma}(z) + z^{-L}H_{a1}(z^{2L})H_{Ma}(z) \tag{26}$$

$$H_{Ma}(z) = \sum_{i=0}^{K-1} z^{-i} E_{Mai}(z^K) \tag{27}$$

Consequently, for the narrowband FRM GDFT-FB the modulated bandpass filters in (22) become

$$H_k(z) = H_{a0}(z^{2L})\sum_{i=0}^{K-1} z^{-i} W_K^{-ki} W_K^{-k_0 i} E'_{Mai}(z^K) + (-1)^k z^{-L} H_{a1}(z^{2L})\sum_{i=0}^{K-1} z^{-i} W_K^{-ki} W_K^{-k_0 i} E'_{Mai}(z^K) \tag{28}$$

where

$$E'_{Mai}(z^K) = E_{Mai}(z^K W_K^{-k_0 D}) \tag{29}$$

For the narrowband FRM GDFT-FB, as for the H-GDFT, there is just one possible value for the interpolation factor L given by (11). Using L, the specifications for the base filter and the positive masking filter may be calculated using Table 1. Comparing (28) with (22), it should be clear that the filter bank must be implemented using the same basic structure (shown in Figure 6) in both the full FRM and narrowband FRM cases.

*B. **Alternative oversampled FRM GDFT-FB***

In the FRM GDFT-FB structure of Figure 6 the base filter is placed before the modulated GDFT-FB structure. Consequently, it must operate at a much higher rate than the masking filter. In addition, when the number of channels, K, is large the base filter interpolation factor, which must comply with (24), requires large zero padding and delay in the base filter polyphase components.

Based on the approach taken in [17], an alternative FRM GDFT-FB structure can be realized. In the alternative structure shown in Figure 7a, the base filter is commuted to the lower sample rate output side of the filter bank using the noble identities. In addition to

performing base filter operations at the lowest sample rate, the interpolation factor applied to the base filter is reduced by a factor equal to the decimation, thereby reducing the zero padding. The structure does, however, require an instance of the commuted base filter on each GDFT-FB output, but this has the benefit that these filters will be real for both even and odd-stacked configurations. This differs from the odd-stacked configuration of the structure in Figure 6 which requires a complex base filter.

For the alternative FRM GDFT-FB to work, the filter bank must be oversampled ($L_{DFT} > 1$) and the oversampling factor L_{DFT} must also be an even number. By applying (10) in (24) and restricting L_{DFT} to an even number bigger than one, it can be seen that the base filter interpolation factor ($2L/D$) and the complementary delays (L/D) in Figure 7a are integers. This structure is not suitable for critically sampled ($L_{DFT} = 1$) filter banks or filter banks with an odd oversampling factor because the base filter interpolation factor would not be an integer.

In the narrowband FRM case, the structure in Figure 7a can be simplified, leading to the more efficient structure shown in Figure 7b. In this variant, the polyphase decomposition of the base filter is avoided, so an interpolated version of the base filter can be used directly. In addition, since the base filter is not divided into polyphase components, symmetry in its coefficients can be exploited to reduce the number of multiplications required.

*C. **Recursive and multi-stage FRM GDFT-FB***

Further reductions in the number of coefficients per filter can be achieved by applying recursive and multi-stage techniques to any of the FRM GDFT-FBs already introduced in this work. The recursive structure consists of a second FRM structure applied to the base filter itself. The increased complexity of the design makes it tedious to implement for the full FRM GDFT-FB but it has been applied to the narrowband FRM GDFT-FB [15].

The recursive narrowband FRM structure is realized by the addition of a second base filter, $H'_a(z^{L'})$, cascaded with the base filter, $H_a(z^L)$, and complementary filters, $H_{Ma}(z)$, as shown in Figure 8a. The second base filter assists the masking filter by eliminating some of the unwanted images arising from interpolation of the first base filter as depicted in Figure 8b. To achieve this, the second base filter's interpolation factor, *L'*, needs to be smaller than *L*. Following the two base filters, a masking filter with a wider transition band (and lower order) than in the normal FRM implementation is used to remove the remaining images of the base filter.

The passband and stopband cut-off frequencies of the (first) base filter are the same as for the normal narrowband FRM implementation given by Table 1. For the recursive (second) base filter $H'_a(z)$ and the masking filter the design specifications are given by

$$\begin{aligned} \theta' &= \omega_p L' \quad \phi' = \left(\frac{2\pi}{L} - \omega_s\right) L' \\ \omega_{Mpa} &= \omega_p \quad \omega_{Msa} = \frac{2\pi}{L'} - \left(\frac{2\pi}{L} - \omega_s\right) \end{aligned} \tag{30}$$

This structure can be integrated into both the basic (Figure 6) and alternative narrowband (Figure 7b) FRM GDFT-FBs already described by adding the second base filter at the input of the filter bank. This new configuration is referred to as the *Recursive FRM GDFT-FB* (R-FRM GDFT).

As an alternative to recursive FRM, multi-stage filtering techniques can be used to reduce the order of the prototype filter in an FRM GDFT-FB. As in [3], the prototype filter specification is relaxed by increasing its transition band to include parts of the adjacent channels. Thereafter, a second stage comprising half-band filters, $H_B(z)$, at the filter bank output eliminates the extra undesired signal, leaving just the desired frequency band. As in [3], it is necessary that the uniform filter bank uses an oversampled configuration

(specifically $L_{DFT} = 2$) in order to be able to use half-band filters at the outputs. Since this multi-stage structure requires oversampling whether using the basic or the alternative narrowband FRM GDFT-FB (Figure 6 and Figure 7b respectively), the multi-stage variant of the alternative narrowband FRM GDFT-FB (M-FRM GDFT) represents the most efficient design in which to apply it.

In FRM designs, passband and stopband ripples from the base filter and masking filter frequency responses both contribute to the final composite frequency response. Because of this the passband and stopband specifications for the base and masking filters must be more stringent than the final filter. According to [20], a useful guideline is to make the base filter passband and stopband ripple and the masking filter passband ripple specifications 20% more stringent than the composite frequency response requires; a masking filter stopband ripple that is 50% more stringent is also recommended.

The R-FRM GDFT and M-FRM GDFT designs are compared by applying them to an eight channel TETRA V&D channelizer, similar to the H-GDFT design example in Figure 5. Since an oversampled configuration ($L_{DFT} = 2$) is required for the M-FRM GDFT, both the R-FRM GDFT and M-FRM GDFT are designed as oversampled to compare their output frequency responses. For both cases the theoretical filter orders are calculated considering the overdesign considerations. For the R-FRM GDFT the filter orders obtained are $N_a = 68$, $N'_a = 22$ and $N_{Ma} = 112$. In this case, the passband and stopband specifications are met at the channelizer outputs. For the corresponding M-FRM GDFT the calculated filter orders are $N_a = 12$, $N_{Ma} = 1362$ and $N_B = 64$, where N_B is the order of the half-band filters. However, for the M-FRM GDFT, with these filter orders the desired output specifications are still not achieved (similar to the H-GDFT) and, therefore, an increase in the half-band filter order to N_B=70 is necessary.

Both frequency responses are shown in Figure 9. Both designs have similar frequency

response in the passband and transition band, but the M-FRM GDFT provides more attenuation in the stopband due to the half-band filter after the filter bank outputs. For both cases the passband peak-to-peak ripple is within the limits. Similar to the H-GDFT in Figure 5, the filter passband magnitude response is not equiripple due to the contribution of several filters to the final frequency response.

D. ***FRM GDFT-FB design examples and computational comparison***

The comparison of the different proposed FRM GDFT-FB designs is based on four factors: filter frequency response, filter orders, group delay, and computational load. In terms of frequency response, the filter bank specifications given in Table 2 for the TETRA V&D and TEDS uniform filter banks are adapted for the FRM GDFT-FB, R-FRM GDFT and M-FRM GDFT channelizers according to the more stringent requirements for FRM designs [20].

Secondly, the filter orders and group delay of each design are compared in Table 3. In it, the order of all filter theoretical orders are calculated following the overdesign considerations expressed in [22]. Group delay calculations masured in number of output samples are also tabulated.

For the full FRM GDFT-FB design, only the calculation of the base (N_a) and masking filters (N_{Ma}, N_{Mc}) orders is required since both masking filters have the same order, N_{Ma}. To calculate the filter orders, first, a particular positive integer value is given to the variable m. This value is used in (24) to obtain the FRM interpolation factor L for either the design case 1 or case 2. Finally, for the chosen design case and the values of m and L, the base and masking filter specifications are given by the expressions in Table 1. In general, according to [24], it has been demonstrated that the variations in the filter specifications and filter orders produced by an increase in the value of m (which implies an increase in L) produces

an increase in the computational load of the FRM GDFT-FB channelizer. In addition, for a given value of *m*, design case 2 leads to smaller computational load than case 1. Therefore, in Table 3 $m = 1$ and case 2 designs are used for the three types of channel.

For the narrowband FRM GDFT-FB there is one single possible value of the interpolation value, L, given by (11). In this design just one base filter, $H_a(z)$, and one masking filter, $H_{Ma}(z)$, are required. Comparing the filter orders for both full FRM GDFT-FB and narrowband FRM GDFT-FB, it can be observed that in general the base filter order (N_a) is larger in the second design. This is a direct consequence of the smaller interpolation factor L employed in the narrowband case, which leads to a base filter specification with a smaller transition band. On the other hand, the masking filter order (N_{Ma}) is generally smaller in the narrowband design since its transition band specification is more relaxed in this case.

The R-FRM GDFT is characterized by the use of one base filter, $H_a(z)$, one recursive base filter, $H'_a(z)$, and one masking filter, $H_{Ma}(z)$. Each of the base filters has its own interpolation factor, L and L' respectively. In this design, the base filter order (N_a) and interpolation factor remain the same as in the narrowband FRM GDFT-FB case since the function of the recursive filter is just to aid the masking filter.

Finally, the M-FRM GDFT does not incorporate a recursive base filter but instead includes a half-band filter, $H_B(z)$, on every output sub-band of the filter bank. The half-band filters allow relaxation of the base filter specifications leading to smaller orders than the narrowband FRM GDFT-FB design. However, the more relaxed interpolated version of the base filter adversely affects the filtering requirements for the masking filter and increases its order in comparison with the narrowband FRM GDFT-FB case.

Table 3 shows that all the FRM methods benefit from significantly shorter individual filters and fewer coefficients in total than the classic GDFT-FB. The smallest saving was

achieved by the full FRM GDFT-FB with up to 50% fewer coefficients, while the R-FRM GDFT provided the largest saving with up to 95% fewer coefficients.

Examining group delay, Table 3 shows that all FRM GDFT-FB channelizers suffer larger group delays than the classic GDFT-FB design for both critically sampled and oversampled configurations. Again, it can be observed how the group delay is proportional to the oversampling factor (L_{DFT}) used in the channelizer. Among the different designs, the narrowband FRM GDFT-FB and R-FRM GDFT provided the smallest group delays.

Despite the significantly reduced filter orders required by the filter bank designs employing the FRM technique, a reduction in their computational load with respect to the classic GDFT-FB cannot be guaranteed. Therefore, a computational analysis comparison of the FRM filter bank designs with the classic GDFT-FB for different use case scenarios is necessary. For this evaluation the TETRA V&D, TEDS 50 kHz and TEDS 100 kHz standards were used. For each filter bank, an odd-stacked uniform channelizer was designed using the filter bank specifications of Table 2 and the filter orders calculated in Table 3. The comparison baseline is the number of real multiplications required per complex input sample. The input of the channelizer is considered to be a wideband complex baseband signal containing all channels. The computational loads for each channelizer are extracted from [8]. In general, the size of the DFT in the GDFT-FB is chosen equal to a power-of-two to permit use of the radix-2 Fast Fourier Transform (FFT). The radix-2 FFT algorithm is considered since it is very commonly implemented in DSP devices such as FPGAs [25]. Nevertheless, all the FRM GDFT-FB designs are independent of the FFT algorithm employed and more efficient algorithms may be employed, such as the Good-Thomas or prime factor algorithm [25], which reduce the computation and do not require a power-of-two DFT size.

Figure 10 presents the computational load differences between the various uniform

channelizer designs. In particular, Figure 10a shows the channelizer options for the critically sampled case. For the FRM methods only the design in Figure 6 is applicable in this situation (for both full and narrowband FRM). Among the critically sampled channelizers, it is apparent that the narrowband FRM GDFT-DB requires most operations per input sample while the full FRM GDFT-FB requires just slightly more than the classic GDFT-FB. The reason for this is the higher order base filter in the narrowband case relative to the full FRM case. This is despite the narrowband FRM GDFT-FB having fewer overall coefficients than the full FRM equivalent (as seen in Table 3). For the structure in Figure 6 the base filter performs at the highest sample rate in comparison with the rest of the filters forming the filter bank. Therefore, small increments in the base filter order represent considerable increments in the computational load.

Finally, Figure 10b shows that when oversampled channelizer configurations are used all the combined FRM and GDFT-FB designs require fewer operations per input sample than the GDFT-FB. In particular, the efficient oversampled narrowband FRM GDFT-FB structure (Figure 7b) requires approximately half the multiplications of the other designs. Moreover, unlike the other oversampled designs, the oversampled narrowband FRM GDFT-FB requires fewer multiplications than any of the critically sampled designs.

IV. Combined FRM and GDFT-FB Designs Applied to Non-Uniform Channelization and DSA

To evaluate non-uniform channelization based on the combined FRM and GDFT-FB designs compared to the GDFT-FB, we consider a DSA use case comprising a mix of TETRA V&D and TEDS channels covering a 5 MHz frequency band as in [8]. The (baseband) multi-channel DSA configuration is always odd-stacked (no channel centred at DC). Three different channel allocation configurations are considered:

- Configuration 1: 100 x 25 kHz TETRA V&D channels, 26 x TEDS 50 kHz channels, and 12 x TEDS 100 kHz channels.
- Configuration 2: 52 x 25 kHz TETRA V&D channels, 50 x TEDS 50 kHz channels, and 12 x TEDS 100 kHz channels.
- Configuration 3: 50 x 25 kHz TETRA V&D channels, 25 x TEDS 50 kHz channels, and 25 x TEDS 100 kHz channels.

Non-uniform channelizers based on the combined FRM and GDFT-FB designs were realized using the same parallel and recombined structures applied to the GDFT-FB (see Figure 11a and Figure 11b) but substituting the appropriate uniform filter bank for the GDFT-FB. The design parameters in Table 1 and filter orders in Table 2 and Table 3 were used for the 25 kHz, 50 kHz and 100 kHz uniform filter banks. The alternative form oversampled narrowband FRM GDFT-FB proved to be the most efficient FRM based uniform design and this design was therefore used as the basis for all FRM configurations evaluated, including the R-FRM GDFT, and M-FRM GDFT.

Figure 11c and Figure 11d shows the results for parallel and recombined filter bank channelizer implementations based on the GDFT-FB and combined FRM and GDFT filter banks for all three channel allocation configurations in the evaluation use case. It is clear that the M-FRM GDFT filter bank is the basis for the most computationally efficient non-uniform channelizers using either the parallel or the recombined filter bank structure. Furthermore, the recombined filter bank structures were all more efficient than their parallel counterparts for the configurations evaluated. In particular, the most efficient recombined M-FRM GDFT channelizer needed up to 60% fewer operations than the corresponding parallel channelizer. In general, all the combined FRM and GDFT designs led to lower computational loads than the Parallel GDFT and Recombined GDFT

implementations using the classic GDFT-FB.

The Parallel R-FRM GDFT is the only exception where no computational reduction is achieved with respect to the classic GDFT-FB implementation. However, this particular filter bank provides the lowest filter orders among all designs, as can be seen in the coefficient calculation in Table 3. Depending on the application, low filter orders can be as important as low computational load. For example, in fixed-point implementations the lower the filter order the less sensitive the frequency response of the filter will be to coefficient quantization errors [26].

In conclusion, the Recombined R-FRM GDFT provides the best overall performance considering both the number of coefficients and computational load. Even though some other designs require fewer operations, the R-FRM GDFT benefits from low filter orders for all the filters composing the channelizer, unlike the other designs which yield a mixture of low order and high order filters. In addition, the R-FRM GDFT employs half-band filters (like all the other FRM GDFT-FB designs) which achieve the required magnitude complementary property required for sub-band recombination automatically.

V. CONCLUSION

In this paper a novel combination of the FRM structure and GDFT-FBs was presented for efficient uniform and non-uniform channelization methods. In particular, two principal approaches were evaluated: cascading the FRM structure with a GDFT-FB and using FRM more directly to implement the GDFT-FB prototype filter more efficiently. Both approaches were analysed for different channel stacking configurations, oversampling factors, and type of FRM (full or narrowband). All of the combined FRM and GDFT-FB structures showed a reduction in the number of coefficients (up to 95%) compared to the basic GDFT-FB implementation. In addition, considering their computational load, all

uniform and non-uniform channelizer designs (with the exception of the uniform FRM GDFT-FB and non-uniform parallel R-FRM GDFT) yielded reductions relative to the basic GDFT-FB based channelizers. However, they all showed larger group delays. Overall, all the combined FRM and GDFT-FB structures presented in this paper outperformed GDFT-FBs in at least one of the comparison parameters, hence leaving the final decision of choosing which structure suits better the purpose of the design to the engineer.

VITAE

Álvaro Palomo-Navarro received his B.Eng. degree in telecommunications engineering from the Polytechnic University of Madrid, Spain, in 2006, and his Ph.D. degree from the National University of Ireland, Maynooth, Ireland, in 2011. Between 2006 and 2007 he worked as a test engineer for GSM intelligent networks. Since 2007 he has worked in the Electronic Engineering Department at the National University of Ireland, Maynooth. His main research interests include multirate DSP, SDR, DSA and multi-standard wireless communications.

Ronan J. Farrell received his B.E. and Ph.D. degrees in electronic engineering from University College Dublin, Ireland, in 1993 and 1998. He is currently a senior lecturer at the National University of Ireland, Maynooth, and director of the Callan Institute for applied ICT. His research interests include physical layer communication technologies, in particular, adaptive receivers, PAs, and active antenna arrays. He is currently the strand leader responsible for radio technologies in the SFI-funded Centre for Telecommunications Research.

Rudi Villing received his B.Eng. degree in electronic engineering from Dublin City University, Ireland, in 1992, and his Ph.D. degree from the National University of Ireland, Maynooth, Ireland, in 2010. He is currently a lecturer at the National University of Ireland, Maynooth, having previously worked in the telecommunications software industry. His research interests include communications and wireless systems (particularly at the interface between the physical infrastructure and the software defined environment) and perceptual signal processing.

REFERENCES

[1] K. C. Zangi and R. D. Koilpillai, "Software radio issues in cellular base stations," *Selected Areas in*

Communications, IEEE Journal on, vol. 17, pp. 561-573, 1999.

[2] T. Hentschel, "Channelization for software defined base stations," *Annales de Telecommunications*, May/June 2002.

[3] A. Palomo Navarro, R. Villing, and R. Farrell, "Practical Non-Uniform Channelization for Multi-standard Base Stations," *ZTE Comms. Journal. Special topic: Digital Front-End and Software Radio Frequency in Wireless Communication and Broadcasting*, vol. 9, December 2011.

[4] E. Hossain, D. Niyato, and D. I. Kim, "Evolution and future trends of research in cognitive radio: a contemporary survey," *Wireless Communications and Mobile Computing*, pp. n/a-n/a, 2013.

[5] F. Khozeimeh and S. Haykin, "Dynamic spectrum management for cognitive radio: an overview," *Wireless Communications and Mobile Computing*, vol. 9, pp. 1447-1459, 2009.

[6] P. Leaves, K. Moessner, R. Tafazolli, D. Grandblaise, D. Bourse, R. Tonjes, and M. Breveglieri, "Dynamic spectrum allocation in composite reconfigurable wireless networks," *Communications Magazine, IEEE*, vol. 42, pp. 72-81, 2004.

[7] A. Boukerche, K. El-Khatib, and T. Huang, "A performance evaluation of distributed dynamic channel allocation protocols for mobile networks," *Wireless Communications and Mobile Computing*, vol. 7, pp. 69-80, 2007.

[8] A. Palomo Navarro, T. Keenan, R. Villing, and R. Farrell, "Non-uniform channelization methods for next generation SDR PMR base stations," in *Computers and Communications (ISCC), 2011 IEEE Symposium on*, 2011, pp. 620-625.

[9] W. A. Abu-Al-Saud and G. L. Stuber, "Efficient wideband channelizer for software radio systems using modulated PR filterbanks," *Signal Processing, IEEE Transactions on*, vol. 52, pp. 2807-2820, 2004.

[10] F. J. M. G. Harris, R., "A receiver structure that performs simultaneous spectral analysis and time series channelization," in *Proceedings of the SDR'09 Technical Conference and Product Exposition*, 2009.

[11] A. Eghbali, H. Johansson, and P. Lowenborg, "Reconfigurable Nonuniform Transmultiplexers Using Uniform Modulated Filter Banks," *Circuits and Systems I: Regular Papers, IEEE Transactions on*, vol. PP, pp. 1-1, 2010.

[12] A. Eghbali, H. Johansson, and P. Lowenborg, "A Farrow-structure-based multi-mode transmultiplexer," in *Circuits and Systems, 2008. ISCAS 2008. IEEE International Symposium on*, 2008, pp. 3114-3117.

[13] R. Mahesh, A. P. Vinod, E. M. K. Lai, and A. Omondi, "Filter Bank Channelizers for Multi-Standard Software Defined Radio Receivers," *Journal of Signal Processing Systems, Springer New York*, 2008.

[14] R. Mahesh and A. P. Vinod, "Reconfigurable Frequency Response Masking Filters for Software Radio Channelization," *Circuits and Systems II: Express Briefs, IEEE Transactions on*, vol. 55, pp. 274-278, 2008.

[15] L. C. R. de Barcellos, "Estruturas Eficientes de Transmultiplexadores e de Bancos de Filtros Modulados por Cossenos," PhD, Electronic Engineering, COPPE/UFRJ, Rio de Janeiro, 2006.

[16] S. L. Netto, P. S. R. Diniz, and L. C. R. Barcellos, "Efficient implementation for cosine-modulated filter banks using the frequency response masking approach," in *Circuits and Systems, 2002. ISCAS 2002. IEEE International Symposium on*, 2002, pp. III-229-III-232 vol.3.

[17] L. Rosenbaum, P. Lowenborg, and H. Johansson, "An approach for synthesis of modulated M-channel FIR filter banks utilizing the frequency-response masking technique," *EURASIP J. Appl. Signal Process.*, vol. 2007, pp. 144-144, 2007.

[18] M. B. Furtado, Jr., P. S. R. Diniz, S. L. Netto, and T. Saramaki, "On the design of high-complexity cosine-modulated transmultiplexers based on the frequency-response masking approach," *Circuits and Systems I: Regular Papers, IEEE Transactions on*, vol. 52, pp. 2413-2426, 2005.

[19] L. Yong, "Frequency-response masking approach for the synthesis of sharp linear phase digital filters," *Circuits and Systems, IEEE Transactions on*, vol. 33, pp. 357-364, 1986.

[20] P. S. R. Diniz, E. A. B. da Silva, and S. L. Netto, *Digital Signal Processing: System Analysis and*

Design: Cambridge University Press, 2002.

[21] H. Johansson, "New classes of frequency-response masking FIR filters," in *Circuits and Systems, 2000. Proceedings. ISCAS 2000 Geneva. The 2000 IEEE International Symposium on*, 2000, pp. 81-84 vol.3.

[22] J. Kaiser, "Nonrecursive Digital Filter Design Using the IO-Sinh Window Function," in *IEEE International Symposium on Circuits and Systems*, 1974.

[23] Q.-G. Liu, B. Champagne, and D. K. C. Ho, "Simple design of oversampled uniform DFT filter banks with applications to subband acoustic echo cancellation," *Signal Processing*, vol. 80, pp. 831-847, 2000.

[24] A. Palomo Navarro, "Channelization for Multi-Standard Software-Defined Radio Base Stations," PhD, Electronic Engineering Dept., National University of Ireland, Maynooth, 2011.

[25] P. Duhamel and M. Vetterli, "Fast fourier transforms: a tutorial review and a state of the art," vol. 19, ed: Elsevier North-Holland, Inc., 1990, pp. 259-299.

[26] J. G. Proakis and D. G. Manolakis, *Digital signal processing: Principles, Algorithms and Applications*: Pearson Prentice Hall, 2007.

TABLE 1
FRM FILTERS SPECIFICATIONS CALCULATION

	Full FRM (Case 1)	Full FRM (Case 2)	Narrowband FRM
Base filter	$\theta = \omega_p L - 2m\pi$ $\phi = \omega_s L - 2m\pi$	$\theta = 2m\pi - \omega_s L$ $\phi = 2m\pi - \omega_p L$	$\theta = \omega_p L$ $\phi = \omega_s L$
Positive Masking filter $H_{Ma}(z)$	$\omega_{Mpa} = \frac{2m\pi + \theta}{L}$ $\omega_{Msa} = \frac{2(m+1)\pi - \phi}{L}$	$\omega_{Mpa} = \frac{2(m-1)\pi + \phi}{L}$ $\omega_{Msa} = \frac{2m\pi - \theta}{L}$	$\omega_{Mpa} = \omega_p$ $\omega_{Msa} = \frac{2\pi}{L} - \omega_s$
Complementary Masking filter $H_{Mc}(z)$	$\omega_{Mpc} = \frac{2m\pi - \theta}{L}$ $\omega_{Msc} = \frac{2m\pi + \phi}{L}$	$\omega_{Mpc} = \frac{2m\pi - \phi}{L}$ $\omega_{Msc} = \frac{2m\pi + \theta}{L}$	n/a

TABLE 2
PROTOTYPE FILTER ORDERS CALCULATED USING H-GDFTS FOR THE SPECIFICATIONS IN [3].

	Number channels (K)	GDFT-FB		H-GDFT	
		Filter order	Group delay*	Filter order	Group delay*
TETRA V&D /TEDS 25 kHz	256	N = 8085	16 / 32	N_a = 64 N = 1294	19 / 38
TEDS 50 kHz	128	N = 3584	14 / 28	N_a = 58 N = 595	17 / 34
TEDS 100 kHz	64	N = 1444	12 / 24	N_a=46 N = 291	14 / 28

* Group delay: Critically sampled (L_{DFT} = 1) configuration / Oversampled by 2 (L_{DFT} = 2) configuration

TABLE 3
PROTOTYPE FILTER ORDERS CALCULATED USING FRMGDFT-FB, R-FRM GDFT AND M-FRM GDFT

	GDFT-FB		FRM GDFT-FB			Narrowband FRM GDFT-FB			R-FRM GDFT			M-FRM GDFT		
	Filter orders	Group delay	Interp. factor	Filter orders	Group delay**	Interp. factor	Filter orders	Group delay*	Interp. factors	Filter orders	Group delay**	Interp. factor	Filter orders	Group delay**
TETRA V&D/ TEDS 25 kHz	N=8085	16 / 32	L=384	N_a=24 N_{Ma}=2043	22 / 44	L=128	N_a=68 N_{Ma}=681	19 / 38	L=128 L'=32	N_a=68 N'_a=22 N_{Ma}=112	- / 38	L=128	N_a=12 N_{Ma}=1362 N_B=64	- / 44
TEDS 50 kHz	N=3584	14 / 28	L=192	N_a=22 N_{Ma}=1022	21 / 42	L=64	N_a=62 N_{Ma}=341	17 / 34	L=64 L'=16	N_a=62 N'_a=22 N_{Ma}=56	- / 35	L=64	N_a=12 N_{Ma}=681 N_B=58	- / 41
TEDS 100 kHz	N=1444	12 / 24	L=96	N_a=16 N_{Ma}=511	16 / 32	L=32	N_a=48 N_{Ma}=171	14 / 28	L=32 L'=8	N_a=48 N'_a=22 N_{Ma}=28	- / 28	L=32	N_a=12 N_{Ma}=341 N_B=46	- / 35

* Group delay: Critically sampled (L_{DFT} = 1) configuration / Oversampled by 2 (L_{DFT} = 2) configuration
** Group delay: Figure 6 implementation (critically sampled L_{DFT} = 1) / Figure 7 implementation (oversampled, L_{DFT} = 2)

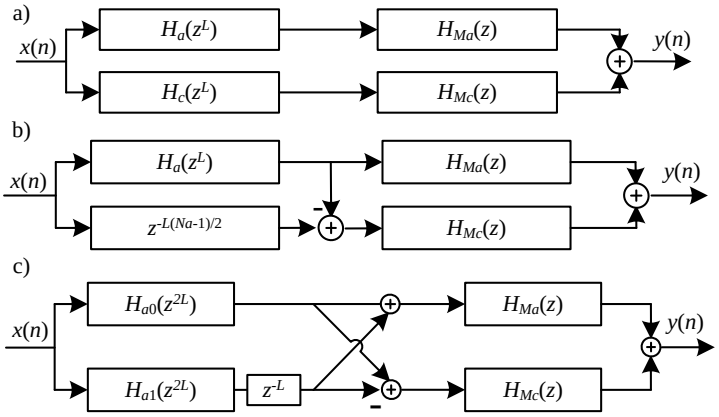

Figure 1 : Frequency response masking. a) Direct implementation, b) efficient implementation, c) polyphase alternative implementation.

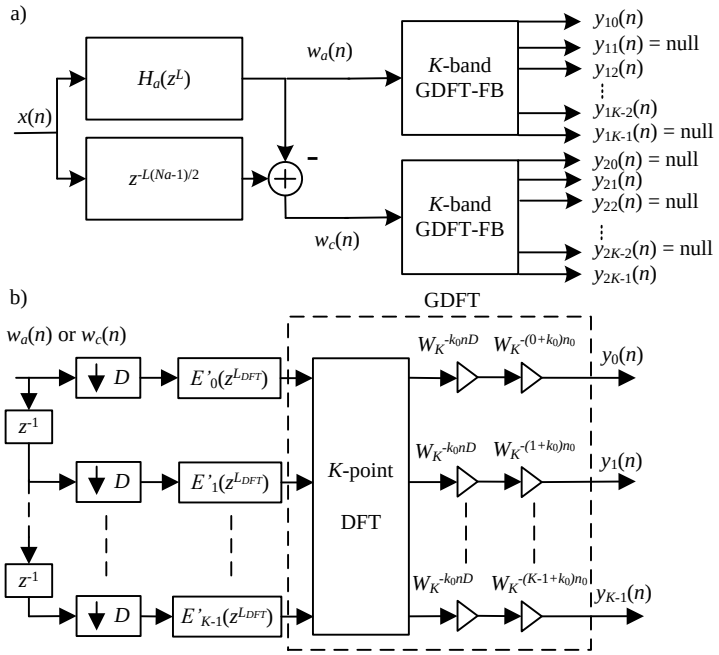

Figure 2 : a) H-GDFT. b) GDFT-FB detail.

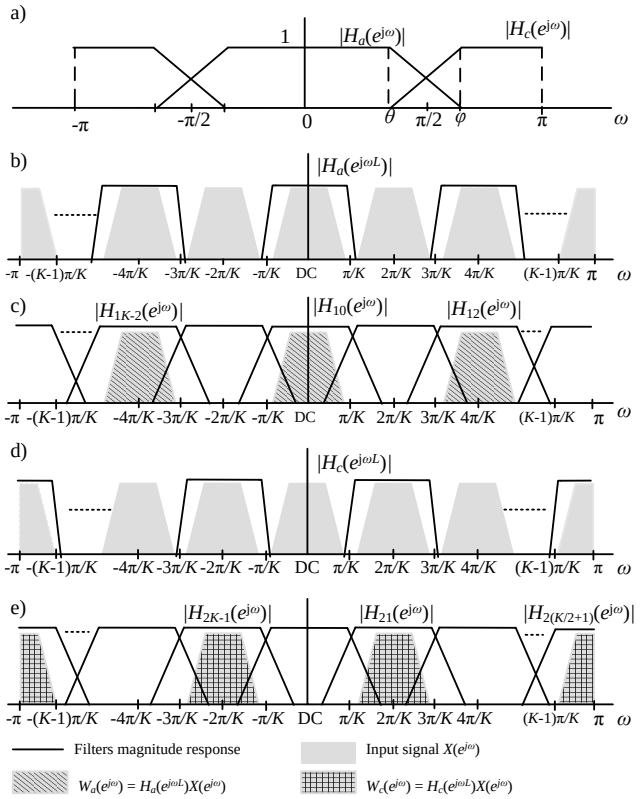

Figure 3 : H-GDFT filtering operations. a) Base filter and complementary filter magnitude responses. b) Even channels filtered by interpolated base filter, c) then filtered by each of the bandpass filters forming the GDFT-FB. d) Odd channels filtered by interpolated complementary filter, e) then filtered by each of the bandpass filters forming the GDFT-FB.

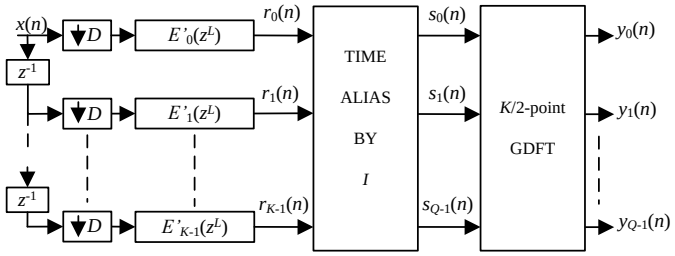

Figure 4 : GDFT-FB with DFT reduction.

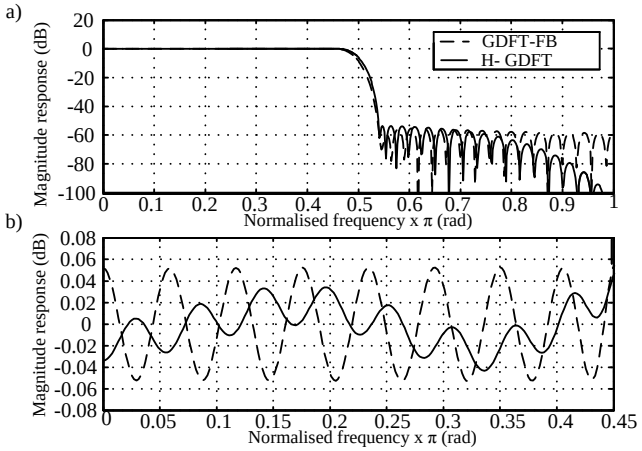

Figure 5 : GDFT-FB and H-GDFT a) output sub-band channel magnitude response for an 8-channel TETRA V&D channelizer, b) bandpass ripple detail.

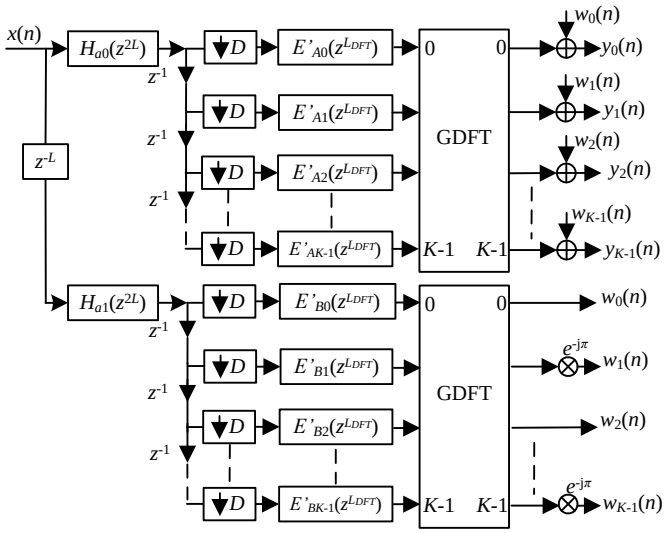

Figure 6 : The GDFT-FB using full FRM.

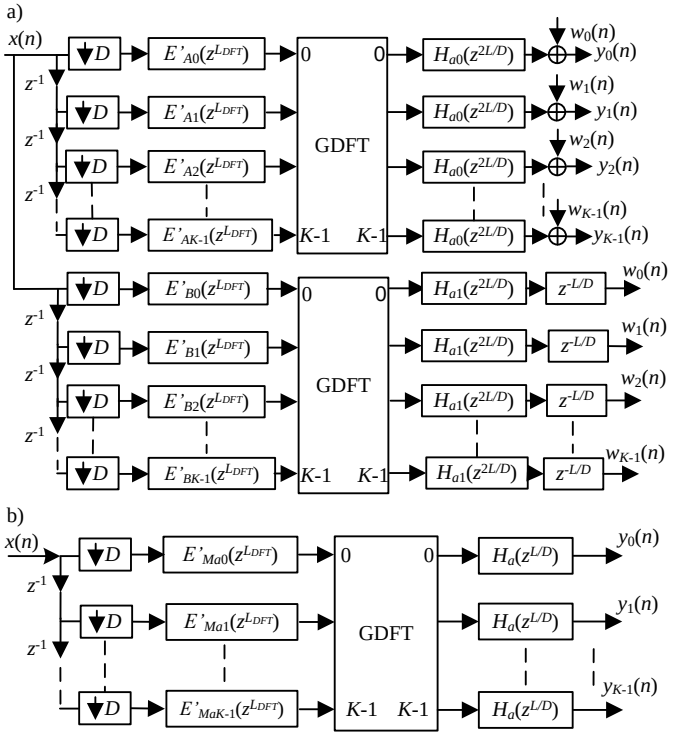

Figure 7 : Alternative structure for a) oversampled full FRM GDFT-FB, b) oversampled narrowband FRM GDFT-FB.

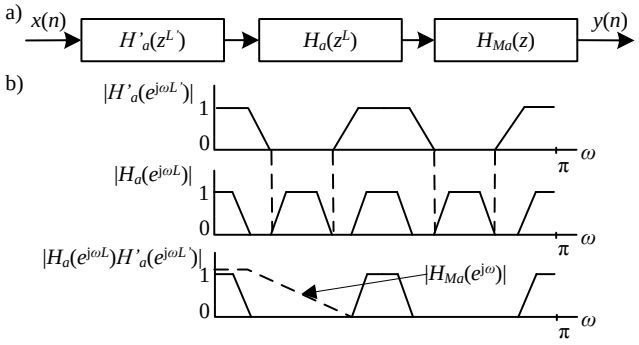

Figure 8 : Recursive narrowband FRM, a) blocks, b) filtering operations.

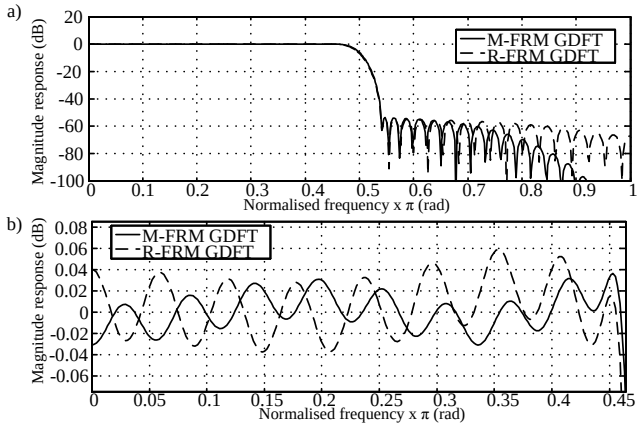

Figure 9 : R-GDFT and M-FRM GDFT a) output sub-band magnitude response for an oversampled 8-channel TETRA V&D channelizer, b) passband detail.

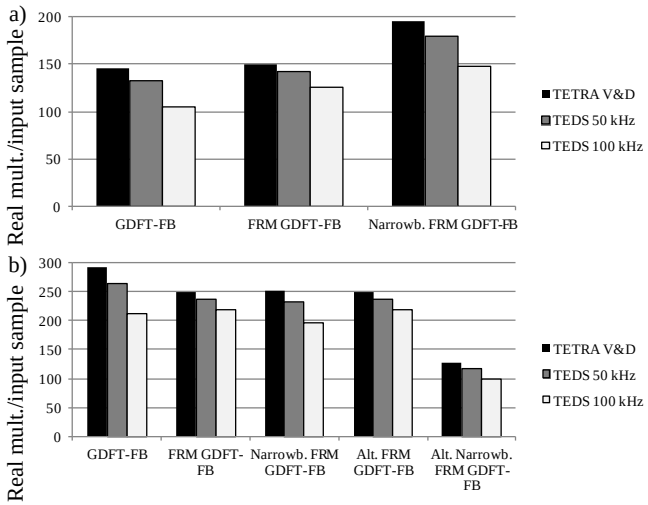

Figure 10 : Computational load of odd-stacked channelizers based on the GDFT-FB and combined FRM and GDFT-FB designs with a) critically sampled configuration, b) oversampled configuration.

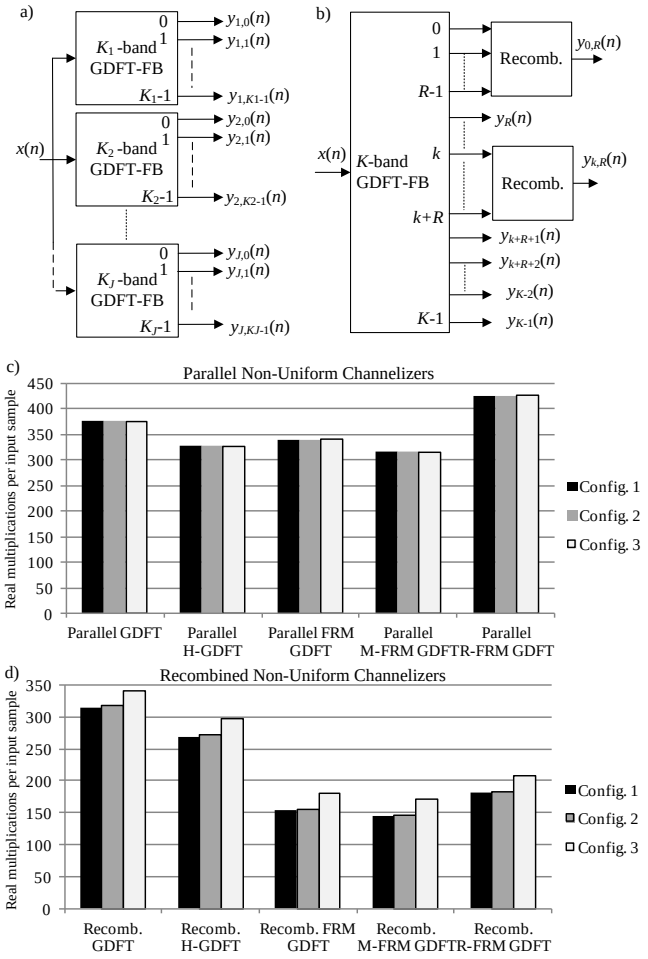

Figure 11 : Non-uniform channelizer. a) Parallel GDFT-FB b) Recombined GDFT-FB. c) Computational load for the three channel configurations for the parallel filter bank structures. d) Computational load for the three channel configurations for the recombined filter bank structures.